Journal of the European Ceramic Society **11** (1993) 95–103

Understanding Nicalon® Fibre

P. Le Coustumer, M. Monthioux & A. Oberlin

Laboratoire Marcel Mathieu, UMR124, 2 av. du Président P. Angot, 64000 Pau, France

(Received 22 January 1992; revised version received 7 April 1992; accepted 11 May 1992)

Abstract

From structural and nanotextural studies by transmission electron microscopy, Nicalon fibre was found to be a microcomposite. Its composition by weight is 55% β-SiC crystals (1·6 nm average diameter), 40% $SiO_{1\cdot15}C_{0\cdot85}$ intergranular phase and 5% free carbon. The free carbon is composed of isolated aromatic entities less than 1 nm in diameter, with 2–3 aromatic layers stacked in turbostratic order. Taking into account the peculiar texture and applying the rule of mixtures, the density and porosity of the as-received fibre have been calculated, and found to be in agreement with measured values. From the nanotextural and chemical events occurring during a series of increasing heat-treatments (argon flow), a chemical balance accounting for the gaseous species released and fibre weight loss is proposed. Qualitative and quantitative changes in elastic modulus and electrical resistivity have been modelled.

Untersuchungen zur Struktur und zur Nanotextur von Nicalon-Fasern mittels Transmissionselektronenmikroskopie zeigen, daß diese Fasern Mikroverbunde darstellen. Sie setzen sich zu 55% aus β-SiC Kristallen (mit einem durchschnittlichen Durchmesser von 1·6 nm), zu 40% aus einer intergranularen Phase der Zusammensetzung $SiO_{1\cdot15}C_{0\cdot85}$ und zu 5% aus freiem Kohlenstoff zusammen, wobei diese Angaben sich als Gewichtsprozente verstehen. Der freie Kohlenstoff besteht aus einzelnen aromatischen Einlagerungen mit weniger als 1 nm Durchmesser und mit 2 bis 3 in turbostratischer Reihenfolge angeordneten aromatischen Schichten. Unter Berücksichtigung dieser speziellen Textur und unter Anwendung der Mischungsregel wurden die Dichte und die Porosität der ursprünglichen Fasern berechnet. Die Rechnungen stehen im Einklang mit experimentell erhaltenen Ergebnissen. Aus der Veränderung der Nanotextur und der Chemie der Fasern nach zunehmender Wärmebehandlung (unter fließendem Argon) konnte die Reaktionsbilanz bezüglich der Entwicklung gasförmiger Spezies und hinsichtlich des Massenverlustes entwickelt werden. Außerdem wurden qualitative und quantitative Veränderungen des Elastizitätsmoduls und des elektrischen Widerstandes simuliert.

L'étude de la structure et de la nanotexture par microscopie électronique à transmission de la fibre Nicalon a permis de l'assimiler à un microcomposite de composition (massique): 55% de cristaux de SiC β(1·6 nm de diamètre moyen), 40% de phase intergranulaire $SiO_{1\cdot15}C_{0\cdot85}$ et 5% de carbone libre. Ce dernier est formé de petites entités aromatiques isolées de moins de 1 nm de diamètre. De cette texture particulière et en appliquant la loi des mélanges, on a calculé la densité et la porosité de la fibre origine, en accord avec les valeurs expérimentales. L'évolution nanotexturale et chimique de la fibre après traitement thermique croissant (sous argon) a permis de reconstituer le bilan réactionnel rendant compte des espèces gazeuses relâchées et de la perte de poids. On a également pu simuler qualitativement et quantitativement les variations des propriétés mécaniques (module d'Young) et électriques (résistivité).

1 Introduction

Despite the abundant literature,[1–11] the precise structure and texture of SiC-based fibres (Nicalon) has not been determined. In addition, neither the quantitative composition of phases, nor the numerical relationship between fibre structure, texture and physical properties has been obtained. Starting from the most recent model available[12] the goal is to complete the characterization in terms of the fibre structure, texture and composition and to interpret fibre properties. The model in Fig. 1 shows both β-SiC microcrystals connected by SiO_xC_y grain boundaries and free carbon whose structure and

Journal of the European Ceramic Society 0955-2219/93/$6.00 © 1993 Elsevier Science Publishers Ltd, England. Printed in Great Britain

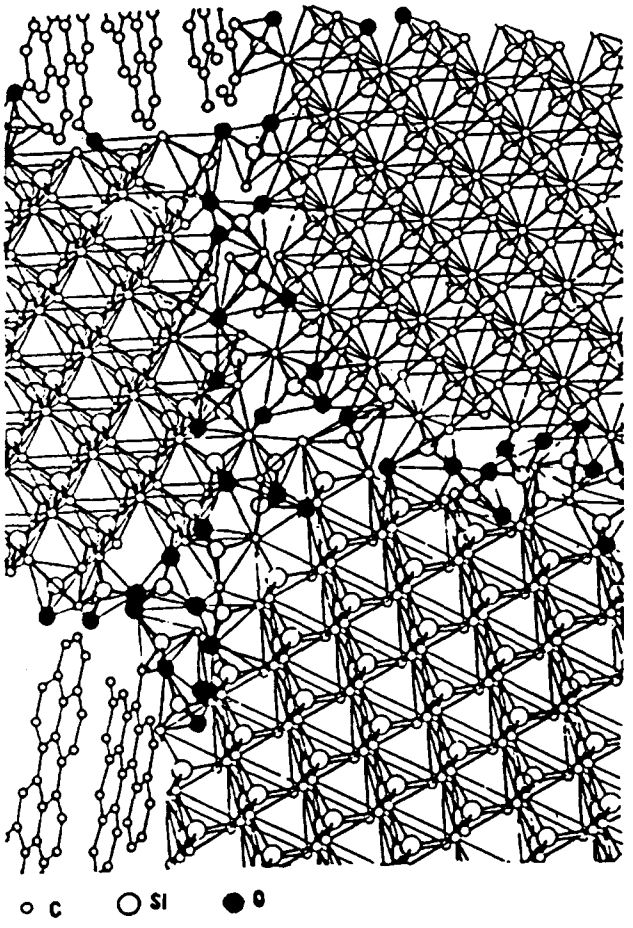

Fig. 1. Model of texture for the as-received Nicalon fibre (from Ref. 12).

orientation are not well determined. The questions left unanswered are:

—What are the quantity, structure and texture of the free carbon?
—What are the stoichiometry and quantity of SiO_xC_y?
—How do these three components behave during thermal treatment, and what are their respective stabilities?
—Is it possible to establish numerical relationships between micro- and nanotextures and physical properties, especially the electrical and mechanical properties?

2 Experimental

The fibre was a ceramic grade Nicalon fibre NLM-202 (Nippon Carbon, Yokohama, Japan), with a polyvinyl acetate size. The size was removed by several washings in warm acetone. Heat treatments were performed in alumina environment (oven walls and crucible) under argon flow (3 litres min^{-1}). Impurities in argon were $O_2 + H_2O < 5$ ppm (volume). Heating rate was 600°C h^{-1} with an isothermal stage of 5 h at the end temperature T_p. T_p ranged from 1000 to 1500°C. The elastic modulus of fibres was measured in tension on single filaments, with a gauge length of 50 mm. Up to twenty tests were made for each sample. Only tests for which an elastic behaviour was obvious were considered. The standard deviations for the E values were ± 10 to ± 30 GPa. Electrical properties were measured following a four-point procedure and using a 617 Keitley-type generator providing a maximal potential of 100 V. At least ten single filaments were tested for each sample, each filament being secured on a Teflon disk with silver paste and maintained under vacuum (133×10^{-4} Pa). Fibre diameters were measured by laser diffractometry.

Samples (single filaments) were prepared by thin sectioning with a diamond knife to obtain thin (< 100 nm) cross-sections of the fibres. The micro- and nanotextures were determined by using all modes of high-resolution transmission electron microscopy (TEM): bright field (BF), dark field (DF), lattice fringes (LF), selected area diffraction (SAD), microdiffraction and X-ray energy dispersive spectroscopy (X-EDS). The X-EDS analysis was performed on a JEOL TEMSCAN 2000 FX equipped with a Si/Li diode (TRACOR) and an ultrathin window (aluminized parylene). Microscopes were Philips CM12 or EM400 (120 kV). Apparent sizes of objective apertures were 2 nm^{-1} for DF mode and 8 nm^{-1} in LF mode. The bulk elemental compositions were determined following a chemical analysis procedure.

3 Results Obtained on the As-received Fibre

3.1 Free carbon

Except in very special cases, described later, the amount of free carbon was not sufficient to yield a detectable pattern in SAD mode. However, when carbon layer stacks occur, they necessarily give rise to faint and widely scattered beams at the 002 Debye–Scherrer ring location. Both carbon 002 dark fields (C_{002} DF) and 002 lattice fringes (C_{002} LF) can be used to detect free carbon. For imaging the carbon layers, the 002 beams scattered by their planes are used, either alone (C_{002} DF), or interfering with the unscattered beam (C_{002} LF). In both cases, only the layer stacks oriented edge-on on the supporting film appear as bright domains or as a set of fringes.

Figure 2 shows a C_{002} DF image full of bright domains, whose size is less than 1 nm (between 0·7 and 0·8 nm). Such observations are valid because the analytical procedure was such that the resolution limit in DF mode was $\delta = 0{\cdot}5$ nm. The orientation of the carbon stacks is random as shown by the similarity of the DF images obtained for any position of the objective aperture along the 002 ring.

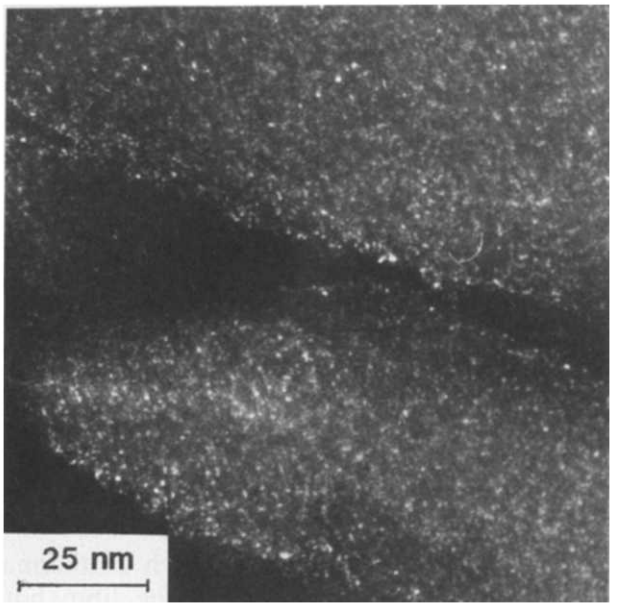

Fig. 2. C_{002} DF image of the as-received Nicalon fibre (bright dots are BSUs).

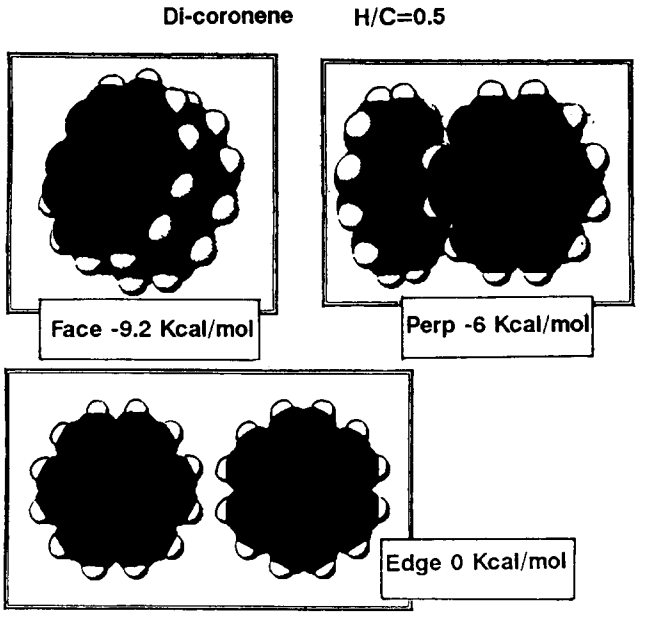

Fig. 4. Possible associations for two coronene molecules (from Ref. 14).

Figure 3 shows a 002 LF image. In this image, small stacks of two fringes (arrowed) appear, the diameters of which are between 0·7 and 0·8 nm. These small units are described as basic structural units (BSUs) i.e. the elemental entities common to many other carbonaceous materials.[13] Due to the low temperature at which the fibre is fabricated, no three-dimensional graphitic order can be present. The systematic occurrence of pairs of fringes in the LF images indicates a face to face association of aromatic ring structures, whereas the BSU diameters suggest a coronene-like molecule. Thermodynamic calculations and computer imaging[14] show that the smallest stable face to face association is the dicoronene (Fig. 4) (below this size, only edge to face is possible). Since no BSU larger than 0·8 nm was found, the suitable model to be adopted is the dicoronene. Its size is 0·74 nm and its H/C atomic ratio is 0·5. For most of carbonaceous materials, $(H/C)_{at} = 0{\cdot}5$ is very frequent near the end of primary carbonization[15] or the end of the oil window in kerogens.[16,17] Considering these data and comparing them to the elemental analysis data (Table 1) for hydrogen (3·7 at.%), the free carbon content is estimated as 7·4 at.% or 5 wt%. This value fits exactly with that obtained from a NMR study.[18]

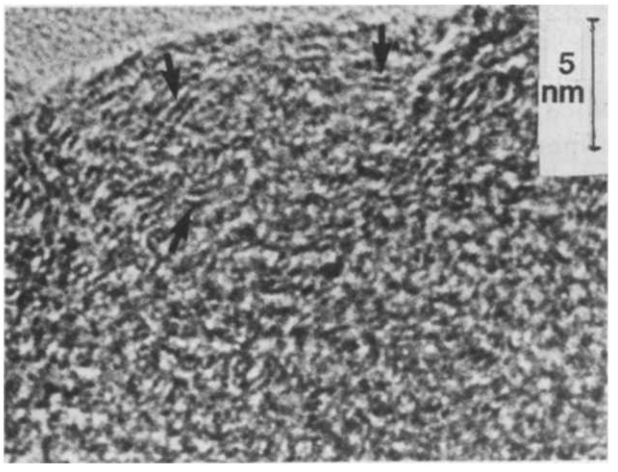

Fig. 3. C_{002} LF of the as-received fibre (arrows indicate BSUs).

3.2 SiO_xC_y continuum and fibre composition

Starting from the elemental analysis data (Table 1), the amount and the formula of this component can be deduced through the following. $a\,SiO_xC_y$: $b\,SiC$:$c\,C$, with (for 100 atoms) $a + b = 37{\cdot}7$, $ax = 15$ and $ay + b + c = 43{\cdot}1$, with $c = 7{\cdot}4$ as calculated in Section 3.1. The SiO_xC_y phase is not seen in SAD patterns, even though overexposed.[19,20] Its amount must be thus minimized, i.e. $(x + y)$ has to be chosen close to 2. The final formula of the fibre in wt% is 55% SiC, 5% C and 40% $SiO_{1{\cdot}15}C_{0{\cdot}85}$. From this composition, the fibre density can be calculated from the respective densities of each phase: 3·2 g cm^{-3} for SiC, 2·2 g cm^{-3} for $SiO_{1{\cdot}15}C_{0{\cdot}85}$ (approximated from amorphous silica), and 2·26 g cm^{-3} for carbon BSUs.[21] The fibre density thus obtained is 2·65 g cm^{-3}. The difference with the value ($d = 2{\cdot}55$ g cm^{-3}) given by the manufacturer (Nippon Carbon data from commercial brochures) may be accounted for by a small amount of porosity ($\sim 2\%$), in accordance with Ref. 10.

3.3 β-SiC

TEM was used to make a size histogram of the β-SiC crystals as measured using DF imaging. However, instead of selecting carbon 002 reflection, the SiC_{111} and/or 220 scattered beams were alternatively used to build the image.[22] The 10 and 11 images of BSU

Table 1. Elemental analysis of the as-received then heat treated Nicalon NL-200 fibre (argon flow, 5 h isothermal)

NL-200 fibre	*Si*		*C*		*O*		*H*		*N*	
	at.%	*wt%*	*at.%*	*wt%*	*at.%*	*wt%*	*at.%*	*wt%*	*at.%*	*wt%*
As-received	37·7	57·9	43·1	28·4	15·0	13·2	3·7	0·2	0·5	0·3
Heat-treated										
1000°C	38·5	58·2	43·9	28·4	15·2	13·1	2·2	0·1	0·3	0·1
1250°C	38·4	57·9	44·3	28·7	15·2	13·2	1·9	0·1	0·1	0·1
1400°C	38·2	57·8	44·2	28·6	15·6	13·4	1·9	0·1	0·1	0·1
1500°C	45·1	65·6	46·3	28·8	6·6	5·4	1·9	0·1	0·1	0·1

still present do not disturb the results because their intensity is negligible. Figure 5(a) shows a SiC_{111} image and Fig. 5(b) shows the corresponding histogram of sizes. The mode is 1 nm, the arithmetic mean is 1·6 nm.

3.4 Conclusion

The Nicalon fibre can be considered as a *microcomposite* comprised of 55 wt% β-SiC microcrystals, 1·6 nm in size, separated from each other by 40 wt% $SiO_{1.15}C_{0.85}$ phase acting as grain boundaries. The 5 wt% free carbon is another intergranular phase made of BSUs located at random. Each BSU is a dicoronene-like molecule. The calculated interlayer spacing[14] is 0·36 nm.

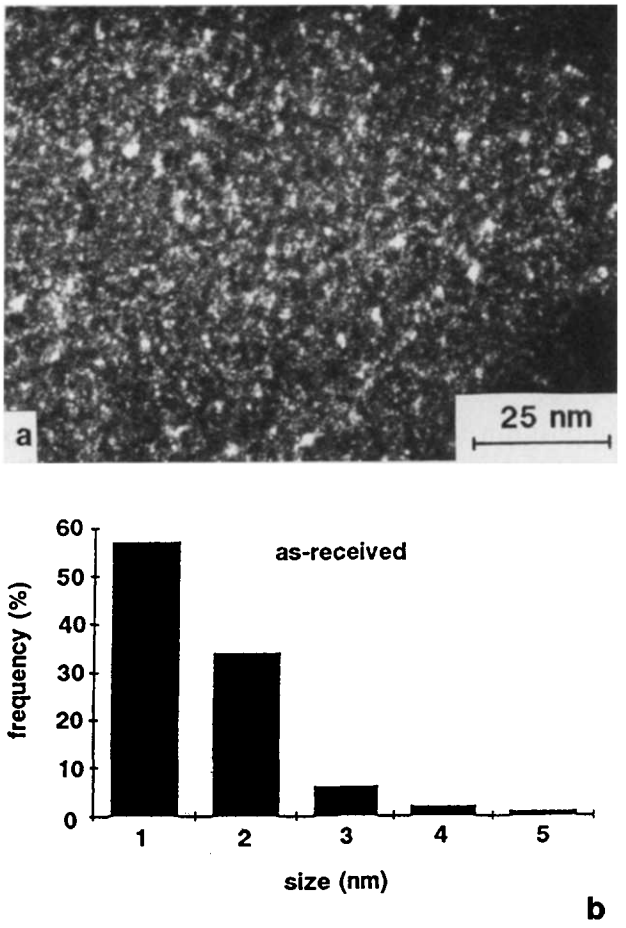

Fig. 5. Size of β-SiC crystals in the as-received Nicalon fibre: (a) SiC_{111} DF image; (b) histogram calculated from (a).

4 Thermal Treatment Under an Inert Gas Flow

The fibres were heat treated under an argon flow ($H_2O + O_2 < 5$ ppm vol.) under various conditions: 1000°C, 1100°C, 1250°C, 1400°C and 1500°C in alumina boats at 600°C/h then 5 h isothermal. Knowing in advance that inside the fibre both free carbon and a potential supply of oxygen ($SiO_{1.15}C_{0.85}$ grain boundaries) coexist, one could expect the occurrence of chemical reactions during subsequent heat treatment. Two overlapping steps can be recognized, the first is still apparent at 1250°C, the final step is completed by 1500°C. An intermediate stage is observed around 1400°C.

4.1 First step (improvement of carbon organization)

In the first step, a very small increase in the mean size of the β-SiC crystals occurs, from 1·6 nm to 2·6 nm (Fig. 6(a)). However, the free carbon is strongly modified. The individual and random BSUs associate with each other edge to edge and form sheets of 4 to 5 distorted layers. The individual BSUs remain as stacks of two superimposed perfect fringes having the length $L1$ corresponding to coronene (~0·7–0·8 nm), whereas their edge to edge association yields distorted fringes having an average length $L2$, ~4 nm (Fig. 7). The distorted layer stacks thus form a more or less contiguous network of open cages around each SiC crystal, as in other SiC-based materials.[23] The lateral bonding between BSUs is a consequence of the release of hydrogen which is completed at 1250°C. This release is shown in Fig. 6(b)) by mass spectrometry analysis. The hydrogen source is the aromatic hydrogen atoms fixed at the periphery of the BSUs. All remaining defects (dangling bonds, hydrogen bonds, sp^3 bonds) are trapped at the BSU boundaries, making the distortions stable and preventing the growth of perfect carbon layers. This step of carbon thermal reorganization is common to many carbonaceous materials. It is also found in the ceramization of polycarbosilanes.[23,24] By considering Fig. 6(b) and (c), it is shown that no other effluent release occurs except hydrogen. Correspondingly the $SiO_{1.15}C_{0.85}$ boundaries are still stable at 1250°C.

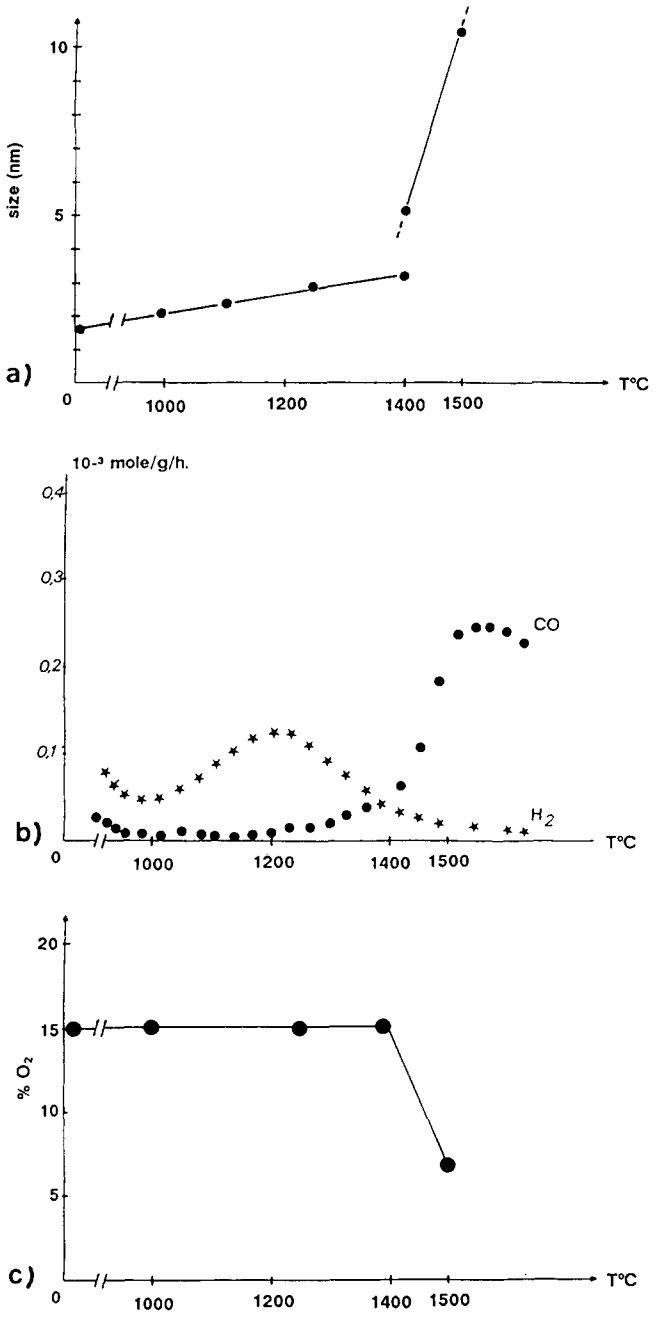

Fig. 6. (a) Mean size of SiC grains versus T_p; (b) release of CO and H_2 as recorded by mass spectrometry; (c) atomic oxygen content of the fibre versus T_p.

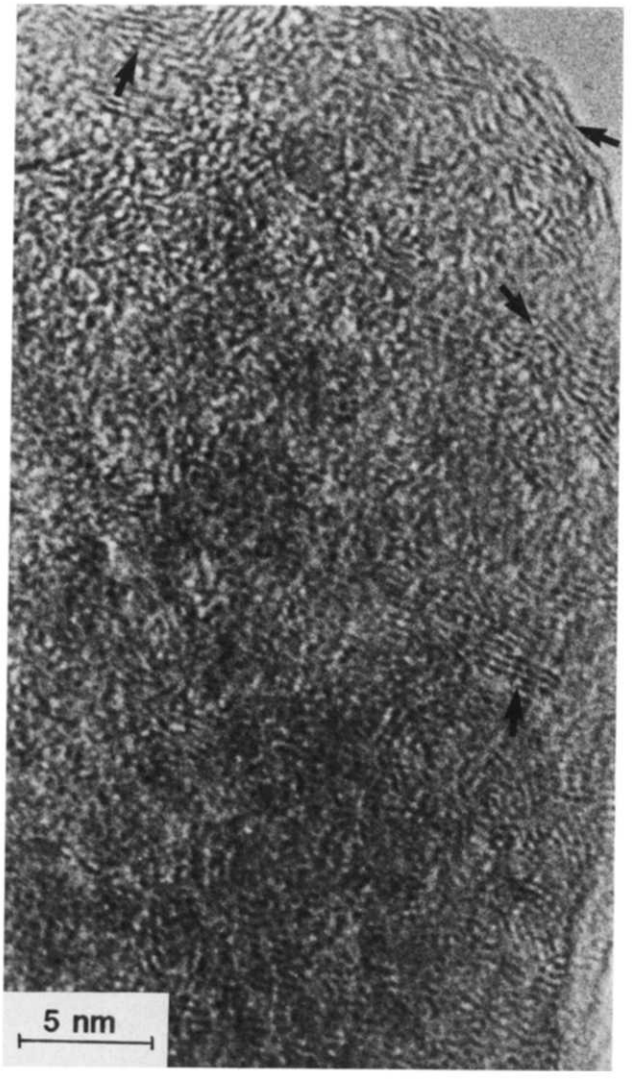

Fig. 7. C_{002} LF image of the Nicalon fibre heat treated within the stability domain (single arrows show BSUs associated edge to edge).

4.2 Final step (grain boundaries degradation)

Figure 8 shows a drastic change in the fibre nanotexture. The β-SiC crystals are now very large (Fig. 6(a)) and the carbon cages are nearly destroyed, or at least strongly degraded. They are either reduced to an isolated BSU (arrows in Fig. 8), or formed into stacks of layers reduced in thickness and having an abnormal spacing (double arrows in Fig. 8). Such a kind of carbon has already been found in some activated carbons with a particularly large specific area.[25] The abnormal spacings are in fact slit pores, caused by the selective oxidation of one aromatic layer in a stack. Individual carbon layers are thus burnt at random in the material. In a more drastic oxidation, whole BSUs are burnt one by one, also at random. The nanotexture of Fig. 8 strongly suggests such an oxidative process. Figure 6(c) shows the strong decrease in the oxygen content of the fibre which begins at 1400°C, and by 1500°C the oxygen content is practically nil. Correspondingly, Fig. 6(b) shows that, after the hydrogen release is complete, a strong maximum in CO release occurs. Simultaneous SiO release was detected but not measured. SiO release has been measured by other authors under similar conditions.[26,27]

The occurrence of two steps in the fibre behaviour is clearly demonstrated, not only by Fig. 6 but also by the grain growth of the SiC (Fig. 9). At 1250°C the histogram of sizes (Fig. 9(a)) is narrow and asymmetrical, whereas it is much wider and symmetrical at 1500°C (Fig. 9(b)).

4.3 Intermediate stage

By considering in more detail Fig. 6(a), one can see that two values of average size are given for SiC crystals at 1400°C. This corresponds to a fibre skin and core effect detected by TEM imaging (Fig. 10(a))

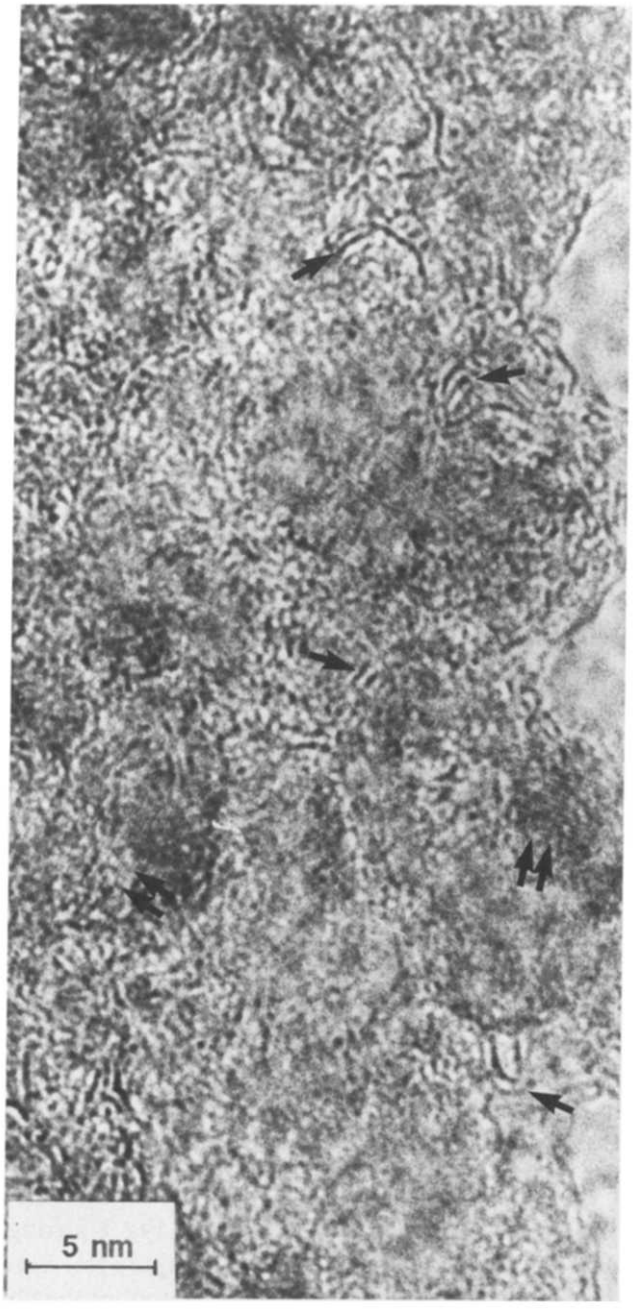

Fig. 8. C_{002} and SiC_{111} LF image of the Nicalon fibre heat treated within the degradation domain (single arrows indicate stacks of distorted carbon layers; double arrows show (111) planes of β-SiC crystals).

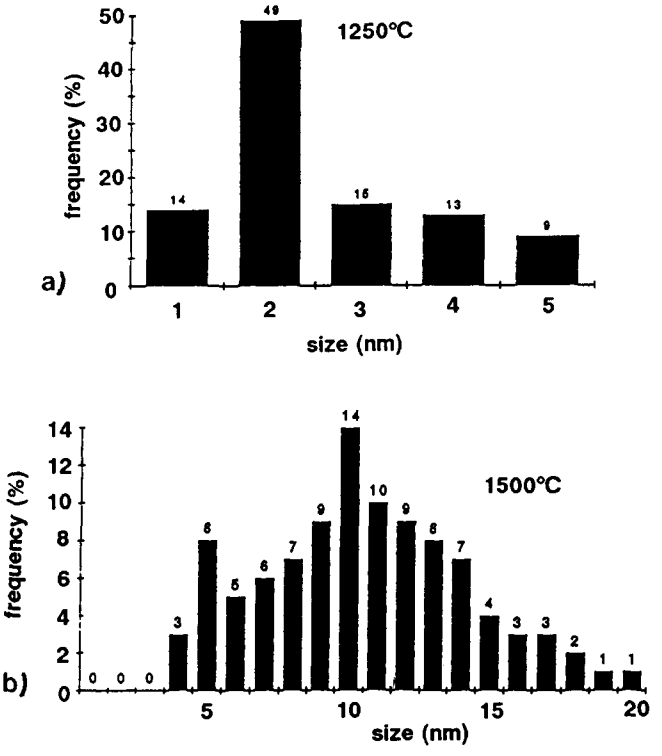

Fig. 9. Size histograms of SiC grains in the heat treated fibre: (a) 1250°C (stability domain); (b) 1500°C (degradation domain).

and SAD (Fig. 10(b) and (c)). The size of SiC crystals from the core has only slightly increased as compared to 1250°C, and the size histogram remains asymmetrical. The carbon layer stacks are intact (Fig. 11). In contrast, the features of the skin (about 0·5 μm in thickness) are similar to that of the bulk at 1500°C. The SiC crystals have grown strongly, and the histograms are symmetrical. The size of the SiC crystals is proportional to the thickness of the skin which increases as the time/temperature conditions increase (Fig. 12). This indicates a diffusion process. Micro-X-EDS measurements were performed respectively on the skin and on the core with a TEM.[21,28] They give an EDS O/Si peak ratio (uncorrected) in the range 0·08–0·11 in the skin versus 0·13–0·14 in the core. At 1500°C, the whole fibre gives O/Si = 0·06–0·07. The gas released is therefore an oxidative species.

4.4 Discussion

The data above necessarily imply the destruction of the $SiO_{1.15}C_{0.85}$ grain boundaries following the reaction:

$$SiO_{1.15}C_{0.85} \rightarrow SiO_{(g)} + 0.15CO_{(g)} + 0.7C_{(s)} \quad (1)$$

further sustained by mass spectrometry data (Fig. 6(b)). The predominance of a SiO species is suggested by NMR data, which found that O is only inserted in –Si–O–Si– and –Si–O–C– bridges in such materials.[29] SiO from reaction (1) is likely to perform a kind of endogeneous oxidation on both the secondary free carbon from reaction (1) and the primary free carbon (carbon network) following the reactions:

$$SiO_{(g)} + 2C_{(s)} \rightarrow SiC_{(s)} + CO_{(g)} \quad (2)$$

These calculations indicate that the fibre (for 100 g) contains 0·7 mol of $SiO_{1.15}C_{0.85}$ and 0·42 mol of primary free carbon. If reactions (1) and (2) are applied, the chemical balance becomes as follows (for 100 g of fibre):

$$0.7SiO_{1.15}C_{0.85(s)} + 0.42C_{(s)} \rightarrow 0.24SiO_{(g)} + 0.56CO_{(g)} + 0.46SiC_{(s)} \quad (3)$$

Reaction (3) can be used to predict the weight loss due to the gaseous CO and excess of SiO released. The calculated value (27%) fits well with experi-

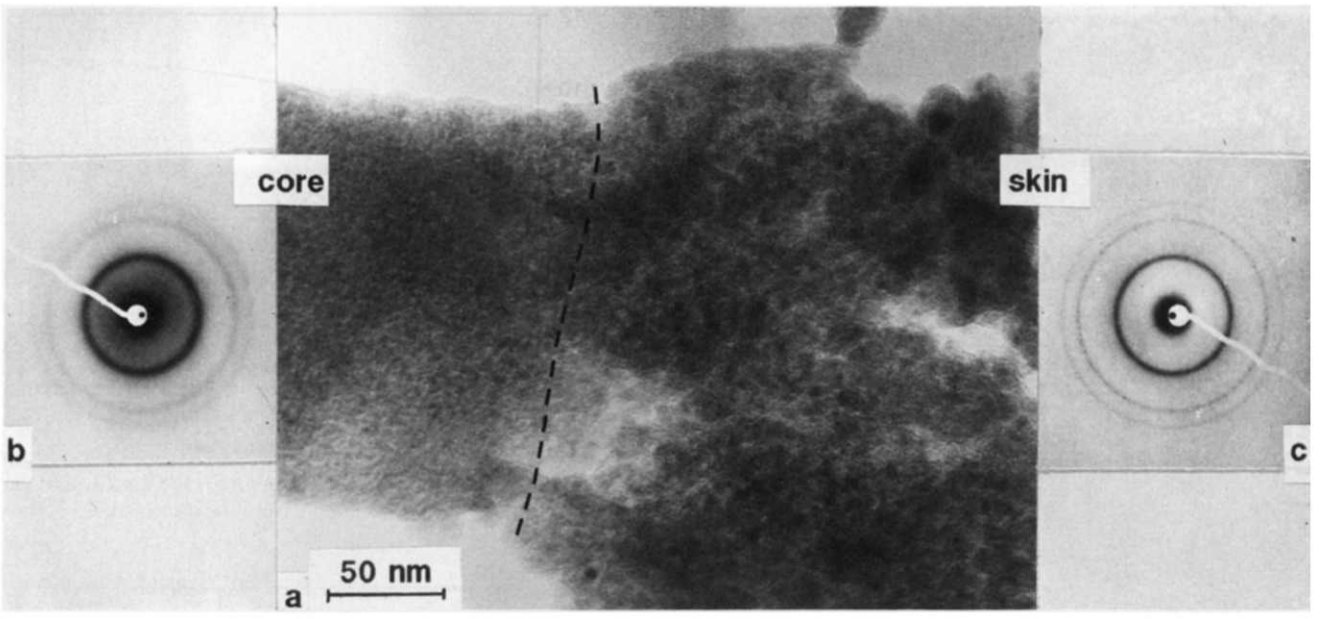

Fig. 10. Skin/core effect in the heat treated Nicalon fibre (intermediate stage): (a) BF image; (b) SAD pattern of the fibre core; (c) SAD pattern of the fibre skin.

mental measurements, i.e. 24%,[30] or 26% (this work, by thermogravimetric analysis up to 1750°C).

As a consequence of reaction (3), secondary SiC becomes available, which probably contributes to the growth of SiC crystals. The presence of excess SiO indicates that SiO from reaction (1) is in excess of the amount required to oxidize all of the free (primary and secondary) carbon. Because both intergranular phases are destroyed, SiC crystals become free to coalesce. Therefore, the main mechanism of growth is a coalescence by impingement, as suggested by the changes in the shape of the histograms.[20,31] The endogeneous oxidation progresses from the surface towards the core of the fibre following the diffusion of gaseous SiO and CO, thereby explaining the skin and core effect.

4.5 Conclusion

In the stability domain of the Nicalon fibre (i.e. the first step), the only change is the edge to edge association of the aromatic free carbon, providing an interconnected carbon network. Afterwards, the fibre degradation is related to an endogeneous oxidation of the carbon phase by gaseous SiO coming from the proper $SiO_{1.15}C_{0.85}$ intergranular phase degradation. A subsequent drastic SiC grain growth occurs, following a coalescence mechanism.

5 Changes in Physical Properties upon Heat Treatment

5.1 Resistivity

In Fig. 13, the resistivity is plotted versus the end temperature T_p. Two changes occur. The first one corresponds to the hydrogen release (Fig. 6(b)). It results (as in other ceramics[23]) from the edge to edge association of the BSUs which were initially isolated and randomly oriented and dispersed. This creates an interconnected network of open cages of carbon around the SiC crystals. The carbon network is a conductor through which the charge carriers can travel. The second decrease in resistivity is related only to the SiC resistivity, since the free carbon is destroyed. The final value tends to that of SiC,[32] since both $SiO_{1.15}C_{0.85}$ and C have disappeared.

5.2 Mechanical properties

Only the Young's modulus was taken into account as an intrinsic property. The experimental values of E versus T_p are plotted in solid line in Fig. 14. The results obtained on the as-received fibre (Section 2) suggest that the fibre can be considered as a microcomposite. Therefore, knowing the molar volume of the various components, an attempt could be made, as a first approximation, to apply the rule of mixtures:

$$E_{\text{fibre}} = E_C \cdot V_C + E_{SiO_xC_y} \cdot V_{SiO_xC_y} + E_{SiC} \cdot V_{SiC}$$

Considering the as-received fibre, the modulus of isolated BSUs can be neglected. The SiC modulus was taken as 400 GPa and the $SiO_{1.15}C_{0.85}$ modulus was chosen as a silica fibre modulus (70 GPa). Taking into account 2 vol.% of porosity, the calculated value for E_{fibre} is 208 GPa.

At 1250°C, the free carbon is optimally organized, i.e. arranged in an interconnected network (see Section 5.1). It is necessary to include its modulus. Since the nanotexture was very similar to that of a high tensile strength PAN-based carbon fibre (first generation),[33] E was chosen as 240 GPa. Correspondingly, the fibre modulus becomes 222 GPa.

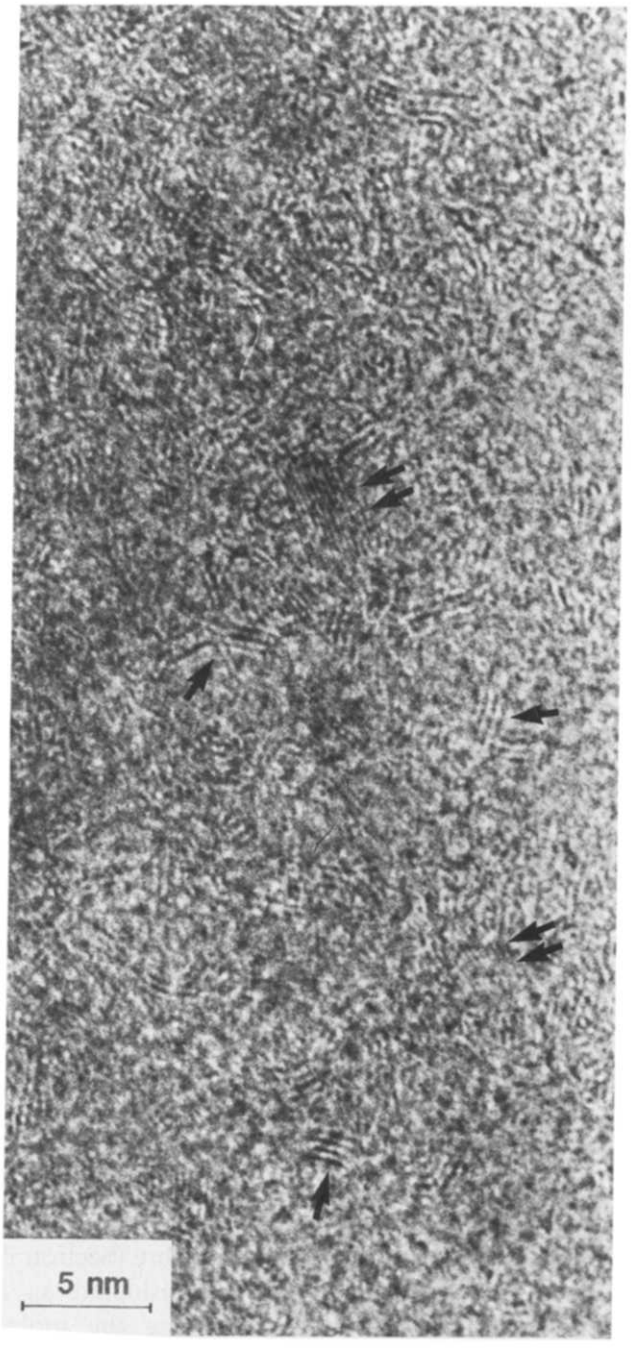

Fig. 11. C_{002} and SiC_{111} LF image of the Nicalon fibre core (intermediate stage). Single arrows indicate walls of the carbon network, double arrows show SiC crystals.

The increase of E in Fig. 14 is thus numerically justified (the calculated values are represented by dotted lines). For 1400°C, it is possible to combine the calculated value for 1250°C with that calculated at 1500°C, assuming the former to be the modulus of the core and the latter the modulus of the skin. Taking into account the respective volumes of the skin and the core at 1400°C as measured by TEM, the 1400°C modulus is 218 GPa (see Fig. 14). At 1500°C, the modulus is calculated assuming an increase in porosity due to the 27% of weight loss (default value because of the unknown shrinkage extent of the fibre). It is found to be 175 GPa.

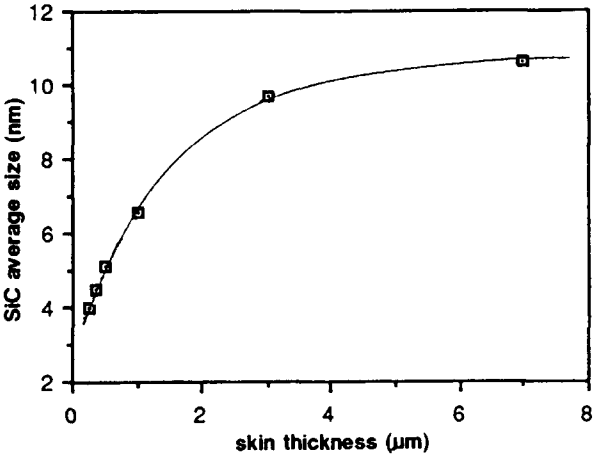

Fig. 12. SiC grain size (mean values) versus the thickness of skin in the Nicalon fibre heat treated within the intermediate domain (from Ref. 21).

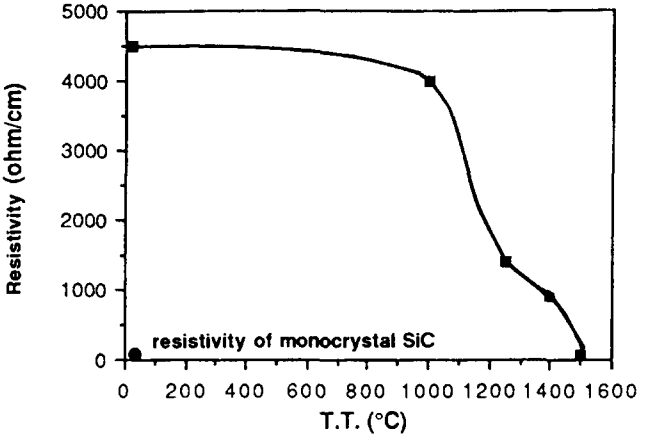

Fig. 13. Changes in the resistivity value of the Nicalon fibre with increasing T_p.

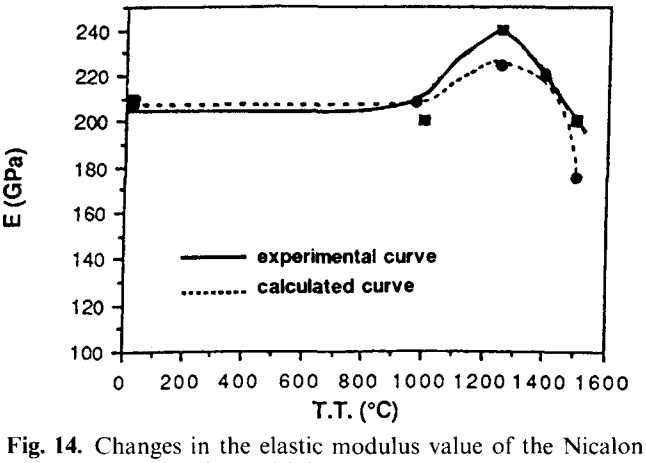

Fig. 14. Changes in the elastic modulus value of the Nicalon fibre with increasing T_p.

5.3 Conclusion

Applying the microcomposite concept to the Nicalon fibre allows the changes in mechanical and electrical properties to be explained, mainly by the changes in the carbon phase nanotexture.

6 General Conclusion

As with many other materials, the physical properties (resistivity and Young's modulus) of the

Nicalon fibre are controlled by the nano- or microtexture. Knowing them well can allow changes in these properties to be understood and predicted qualitatively as well as quantitatively. Of course, approximations have had to be used in this paper. However, the data fit sufficiently well to yield satisfactory interpretations. From a mechanical point of view, it is obvious that the role of free carbon, contrarily to that of the intrinsic O, is beneficial to the fibre.

Acknowledgements

The authors thank Rhône-Poulenc for providing analytical data and financial support, F. Cortial (E.C.N., Nantes, France) for help with X-EDS analysis, and B. Maruyama for linguistic advice.

References

1. Yajima, S., Okamura, K. & Hayashi, J., Structural analysis in continuous silicon carbide fiber of high tensile strength. *Chem. Lett.*, (1975) 1209–12.
2. Yajima, S., Okamura, K. & Hayashi, J. & Omori, M., Synthesis of continuous SiC fibers with high tensile strength. *J. Am. Ceram. Soc.*, **59** (1976) 324–7.
3. Yajima, S., Hayashi, J., Omori, M. & Okamura, K., Development of a silicon carbide fibre with high tensile strength. *Nature*, **261** (1976) 683–5.
4. Yajima, S., Okamura, K., Matsuzawa, T., Hasegawa, J. & Shishido, T., Anomalous characteristics of the microcrystalline state of SiC fibres. *Nature*, **279** (1979) 706–7.
5. Anderson, C. H. & Warren, R., Silicon carbide fibres and their potential for use in composite materials, Part 1. *Composites*, **15** (1984) 16–24.
6. Simon, G. & Bunsell, A. R., Mechanical and structural characterization of the Nicalon silicon carbide fibre. *J. Mater. Sci.*, **19** (1984) 3649–57.
7. Mah, T., Hecht, N. L., McCullum, D. E., Hoenigman, J. R., Kim, H. M., Katz, A. P. & Lipsitt, H. A., Thermal stability of SiC fibres (Nicalon). *J. Mater. Sci.*, **19** (1984) 1191–201.
8. Clark, T. J., Aarons, R. M., Stamatoff, J. B. & Rabe, J., Thermal degradation of Nicalon SiC fiber. *Ceram. Eng. Sci. Proc.*, **6** (1985) 546–58.
9. Sawyer, L. C., Chen, R. T., Haimbach IV, F., Harget, P. J., Prack, E. R. & Jaffe, M., Thermal stability characterization of SiC ceramic fibers: II. Fractography and structure. *Ceram. Eng. Sci. Proc.*, **7** (1986) 914–29.
10. Lipowitz, J., Freeman, H. A., Chen, R. T. & Prack, E. R., Composition and structure of ceramic fibers prepared from polymer precursors. *Adv. Ceram. Mater.*, **2** (1987) 121–8.
11. Porte, L. & Sartre, A., Evidence for a silicon oxycarbide phase in the Nicalon silicon carbide fibre. *J. Mater. Sci.*, **24** (1989) 271–86.
12. Laffon, C., Flanck, A. M., Lagarde, P., Laridjani, M., Hagège, R., Olry, P., Cotteret, J., Dixmier, J., Miquel, J. L., Hommel, H. & Legrand, A. P., Study of Nicalon-based ceramic fibres and powders by EXAFS spectrometry, X-ray diffractometry and some additional methods. *J. Mater. Sci.*, **24** (1989) 1503–12.
13. Oberlin, A., High resolution TEM studies of carbonization and graphitization. In *Chemistry and Physics of Carbon*, Vol. 22, ed. P. A. Thrower. Marcel Dekker, New York & Basel, 1989, pp. 1–143.
14. Vorpagel, R. E. & Lavin, J. G., Most stable configurations of molecules in pitches via molecular modelling, *Carbon* (submitted).
15. Pelet, R., Behar, F. & Monin, J. C., Resins and asphaltenes in the generation and migration of petroleum. In *Advances in Organic Geochemistry 1985*, ed. D. Leythaeuser & J. Rullkötter. Pergamon Press, Oxford, 1986, pp. 481–98.
16. Boulmier, J. L., Oberlin, A. & Durand, B., Structural study of some series of kerogens and relation to carbonization process (high resolution electron microscopy). In *Proceedings of the 7th International Meeting of Organic Geochemistry*, ed. R. Campos & J. Goni. ENADIMSA, Madrid, 1977, pp. 781–96.
17. Oberlin, A., Villey, M. & Combaz, A., Pyrolysis mechanism as studied by electron microscopy, DTA, IR and ESR. *Carbon*, **16** (1978) 73–4.
18. Hommel, H., Miquel, J. L. & Legrand, A. P., Apports de la R.M.N. du solide à l'étude de fibres de carbure de silicum. *L'Indust. Ceram.*, **849** (1990) 1–3.
19. Maniette, Y. & Oberlin, A., TEM characterization of some crude or air heat-treated SiC Nicalon fibres. *J. Mater. Sci.*, **24** (1989) 3361–70.
20. Le Coustumer, P., Monthioux, M. & Oberlin, A., Mécanisme de dégradation d'une fibre Nicalon série 200. In *Actes du Colloque AMAC-CODEMAC Matériaux composites pour applications à hautes températures*, Bordeaux, ed. R. Naslain, J. Lamalle & J. L. Zulian. AMAC, Paris, 1990, pp. 43–53.
21. Le Coustumer, P., Etude du système Si–O–C, exemple de la fibre Nicalon série 200. Mécanismes d'évolution et de dégradation sous différentes atmosphères. PhD Thesis, Université de Pau et des Pays de l'Adour, France, 1991.
22. Ayache, J., Bonnamy, S., Bourrat, X., Deurbergue, A., Maniette, Y., Oberlin, A., Bacque, E., Bro, M., Dunogues, J. & Pillot, J. P., Characterization of some pyrolysed polycarbosilanes by transmission electron microscopy. *J. Mater. Sci. Lett.*, **7** (1988) 885–90.
23. Monthioux, M., Oberlin, A. & Bouillon, E., Relationship between microtexture and electrical properties during heat-treatment of SiC fibre precursor. *Comp. Sci. Technol.*, **37** (1990) 21–37.
24. Delverdier, O., Monthioux, M. & Oberlin, A., Rôle de l'oxygène dans l'évolution thermique de céramiques issues de polycarbosilanes. In *Comptes-Rendus des Septièmes Journées Nationales sur les Composites*, ed. G. Fantozzi & P. Fleischmann. AMAC, Paris, 1990, pp. 103–11.
25. Huttepain, M. & Oberlin, A., Microtexture of nongraphitizing carbons and TEM studies of some activated samples. *Carbon*, **28** (1990) 103–11.
26. Luthra, K. L., Thermochemical analysis of the stability of continuous SiC fibers. *J. Am. Ceram. Soc.*, **69** (1986) C-231–C-233.
27. Johnson, S. M., Brittain, R. D., Lamoreaux, R. H. & Rowcliffe, D. J., Degradation mechanisms of silicon carbide fibers. *J. Am. Ceram. Soc.*, **71** (1988) C-132–C-135.
28. Le Coustumer, P., Monthioux, M. & Oberlin, A., Thermal degradation mechanisms of a Nicalon fiber as deduced from TEM observations. In *Extended Abstracts of International Symposium on Carbon*, Vol. 1. Tanso, Tsukuba, 1990, pp. 182–5.
29. Taki, T., Okamura, K. & Sato, M., A study of the oxidation curing mechanisms of polycarbosilane fibre by solid-state high-resolution nuclear magnetic resonance. *J. Mater. Sci.*, **24** (1989) 1263–7.
30. Filipuzzi, L., Oxydation des composites SiC/SiC et de leurs constituants: approche expérimentale, modélisation et influence sur le comportement mécaniques. PhD Thesis, Université de Bordeaux I, France, 1991.
31. Métois, J. J., Zanghi, J. C., Erre, R. & Kern, R., Coalescence par chocs intergranulaires dans les couches minces (cas de l'or sur (100) KCl). *Thin Solid Films*, **22** (1974) 331–50.
32. Richerson, D. W., In *Modern Ceramic Engineering*, ed. G. Boothroyd & G. E. Dieter. Marcel Dekker, New York, 1982, pp. 46–7.
33. Guigon, M., Oberlin, A. & Desarmot, G., Microtexture and structure of some high tensile strength, PAN-based carbon fibres. *Fibre Sci. Technol.*, **20** (1984) 55–72.